ICCFD13 MILAN ITALY 2026

ICCFD13-2026-366

Implementation of a Wall-Modeled Implicit LES in a discontinuous Galerkin Solver

F. Mangini*, F. Massa*, A. Crivellini** and A. Colombo*
Corresponding author: francesco.mangini@unibg.it
Other authors: {alessandro.colombo,francescocarlo.massa}@unibg.it,
a.crivellini@staff.univpm.it
* University of Bergamo,
Department of Engineering and Applied Sciences,
viale Marconi 20, Dalmine (BG), 24044, Italy.
** Polytechnic University of Marche,
Department of Industrial Engineering and Mathematical Sciences
via Brecce Bianche 12, Ancona, 60131, Italy.

Abstract: This work presents the implementation and assessment of a Wall-Modeled implicit Large-Eddy Simulation (WMiLES) strategy within an entropy-stable modal discontinuous Galerkin (dG) solver for the compressible Navier–Stokes equations. The approach is motivated by the prohibitive cost of wall-resolved LES at high Reynolds numbers, where the near-wall resolution requirements severely constrain both the number of degrees of freedom and the admissible time step for explicit time-integrators. In the proposed formulation, the no-slip wall condition is replaced by a slip condition coupled with modeled wall shear stress and heat flux contributions, imposed through the viscous flux. The underlying high-order dG framework employs an orthonormal modal basis in physical space, advances the conservative variables explicitly in time, and assembles the spatial residual using a projection of the conservative variables onto entropy variables. The Direct Enforcement of Entropy Balance correction is used to recover the desired discrete entropy behaviour without numerical over-integration. Different wall-modelling strategies are considered. Algebraic laws based on the Reichardt velocity profile and Kader temperature law are first introduced. In addition, first results using ODE-based wall models discretized through a one-dimensional dG formulation along wall-normal segments connecting each wall quadrature point to its donor location are presented. The numerical results include the inviscid Taylor–Green vortex test case, used to highlight the entropy conservation/stability properties of the scheme, and the turbulent channel-flow case at $Re_\tau = 2000$, used to evaluate the proposed WMiLES implementation.

Keywords: Wall-Modeled iLES, discontinuous Galerkin methods, Entropy-Stable Schemes.

1. Introduction

The efficient scale resolving simulation of turbulent flows at high Reynolds numbers represents one of the most relevant open challenges in Computational Fluid Dynamics (CFD) applied to engineering and industrial aerodynamics. In current industrial practice, aerodynamic design still relies mainly on methodologies based on the solution of the Reynolds-Averaged Navier-Stokes (RANS) equations. Although RANS models ensure a sustainable computational cost, they exhibit strong predictive limitations and a marked lack of accuracy in complex flow regimes typical of real-world applications, such as massively separated flows [1]. Conversely, scale-resolving simulation techniques, including Large-Eddy Simulation (LES), offer a significantly higher level of fidelity, capturing the intrinsic physics of unsteady flows and multi-scale vortex structures. However, extending LES to high-Reynolds-number flows remains prohibitive for routine scientific computing. This limitation stems from the stringent spatial and temporal resolution required to properly capture the inner part of the boundary layer, where grid requirements scale as $Re^{13/7}$ [2]. Consequently, to perform Wall Resolved LES (WRLES) of wall-bounded flows, the majority of degrees of freedom need to be clustered near the wall, limiting its applicability to low-Reynolds-number regimes [3].

To mitigate this computational cost, the Wall-Modeled LES (WMLES) approach emerges as one of the most promising strategies. The WMLES methodology avoids the computationally expensive resolution of the inner sublayer of the viscous boundary layer. Over the years, wall-modeling strategies have been extended to different numerical frameworks, including finite-element discretizations [4] and dG [5], and have also been applied to high-Reynolds-number simulations of aerodynamic configurations [6]. More recently, generalized wall-modeling strategies have been developed with the aim of addressing complex industrial applications [7]. Instead of imposing the classical no-slip condition, this approach prescribes a slip wall condition coupled with a modeled wall shear stress τ_w directly at the wall. This stress is derived analytically or numerically by reconstructing the local velocity profile from flow variables sampled at a specified distance from the wall, known as the donor location.

In this scenario, high-order dG methods prove particularly well-suited for the implicit Large-Eddy Simulation (iLES) of compressible turbulent flows, as their intrinsic numerical dissipation effectively acts as an underlying SubGrid-Scale (SGS) model, preserving the resolution of macroscopic structures [8]. In addition, recent applications of wall-modeled LES based on high-order dG/DGSEM discretizations have shown the potential of this class of methods for complex aerodynamic configurations [9].

However, standard high-order dG formulations are known to be sensitive to under-resolved flow features and strong gradients [10]. In such regimes, additional stabilization, limiting, or shock-capturing mechanisms are often required to obtain robust computations. To address these issues, an entropy-stable modal dG framework has recently been developed [11, 12]. In this approach, the residual of the spatial discretization is assembled for the L_2-projection on entropy variables as proposed in [13], while the Direct Enforcement of Entropy Balance (DEEB) [14] is employed to satisfy the entropy balance at the discrete level without the need for numerical over-integration. Since the solution is advanced in terms of the degrees of freedom of the conservative variables, explicit time-integration schemes, such as Strong Stability Preserving Runge–Kutta methods [15], can be used without requiring the solution of linear systems [11]. This feature makes the framework particularly suitable for a wall-modeled iLES formulation. Indeed, by allowing the use of significantly coarser wall-normal resolutions than wall-resolved LES, WMiLES reduces both the number of degrees of freedom in the near-wall region and the severe time-step restrictions typically associated with explicit schemes [16]. The resulting approach therefore combines the robustness of the entropy-stable dG discretization with the computational efficiency gained by modeling the innermost part of the boundary layer.

On this basis, the present work focuses on the implementation and assessment of such a strategy. The paper is organized as follows. Section 2 introduces the governing equations and the numerical framework. Section 3 describes the wall-model implementation, considering both algebraic wall laws and Ordinary Differential Equation (ODE)-based wall models. Section 4 presents the numerical results. The inviscid Taylor–Green vortex is first considered to assess the entropy conservation/stability properties of the scheme. Then, turbulent channel-flow simulations at $Re_\tau = 2\,000$ are used to evaluate the proposed WMiLES implementation. Finally, Section 5 summarizes the main conclusions and outlines possible future developments.

2. Governing equations and numerical framework

We consider the compressible Navier–Stokes equations for a calorically perfect gas in a d-dimensional space. In conservative form they are expressed as

$$\frac{\partial \rho}{\partial t} + \frac{\partial (\rho u_j)}{\partial x_j} = 0, \tag{1}$$

$$\frac{\partial(\rho u_i)}{\partial t} + \frac{\partial(\rho u_i u_j + p\delta_{ij})}{\partial x_j} = \frac{\partial \tau_{ij}}{\partial x_j}, \tag{2}$$

$$\frac{\partial(\rho E)}{\partial t} + \frac{\partial\left[(\rho E + p)u_j\right]}{\partial x_j} = \frac{\partial}{\partial x_j}\left(u_i\tau_{ij} - q_j\right), \tag{3}$$

where ρ, $\mathbf{u} = [u_1, \ldots, u_d]^\top$, p, and $E = e + \|\mathbf{u}\|^2/2$ are density, velocity vector, pressure, and total specific energy, respectively. The viscous stress tensor τ_{ij} and the heat flux vector q_j are modeled as

$$\tau_{ij} = \mu\left(\frac{\partial u_i}{\partial x_j} + \frac{\partial u_j}{\partial x_i}\right) + \lambda\frac{\partial u_k}{\partial x_k}\delta_{ij}, \qquad q_j = -\hat{k}\frac{\partial T}{\partial x_j}, \tag{4}$$

where $\lambda = -2\mu/3$, μ is the dynamic viscosity, and $\hat{k} = \mu c_p/Pr$ is the thermal conductivity. The system is closed by the ideal gas equation of state $p = (\gamma - 1)\rho e$, where γ is the heat capacity ratio. By defining the vector of conservative variables $\mathbf{q} = [\rho,\ \rho u_1,\ \ldots,\ \rho u_d,\ \rho E]^\top \in \mathbb{R}^{(2+d)}$, the system can be compactly rewritten as

$$\frac{\partial \mathbf{q}}{\partial t} + \frac{\partial \mathbf{F}_{c,i}(\mathbf{q})}{\partial x_i} + \frac{\partial \mathbf{F}_{v,i}(\mathbf{q}, \nabla\mathbf{q})}{\partial x_i} = \mathbf{0}, \tag{5}$$

where $\mathbf{F}_{c,i}$ and $\mathbf{F}_{v,i}$ represent the inviscid and viscous fluxes. For the spatial discretization, the computational domain Ω is partitioned into a tessellation $\mathcal{K}_h$ of non-overlapping elements K, and the set of mesh faces $\mathcal{F}_h = \mathcal{F}_h^0 \bigcup \mathcal{F}_h^b$, partitioned into subset of internal $\mathcal{F}_h^0$ and boundary $\mathcal{F}_h^b$ faces. Multiplying Eq. (5) by a smooth test function $\mathbf{\Phi} \in \mathbb{R}^{2+d}$ and integrating by parts yields the weak formulation

$$\begin{aligned}\int_\Omega \mathbf{\Phi}^\top \frac{\partial \mathbf{q}}{\partial t} d\Omega - \int_\Omega \left(\frac{\partial \mathbf{\Phi}}{\partial x_i}\right)^\top \left(\mathbf{F}_{c,i}\left(\mathbf{q}\right) + \mathbf{F}_{v,i}\left(\mathbf{q}, \nabla\mathbf{q}\right)\right) d\Omega \\ + \int_{\partial\Omega} \mathbf{\Phi}^\top \left(\mathbf{F}_{c,i}\left(\mathbf{q}\right) + \mathbf{F}_{v,i}\left(\mathbf{q}, \nabla\mathbf{q}\right)\right) n_i \, d\sigma = 0,\end{aligned} \tag{6}$$

where n_i is the unit normal vector pointing out from $\partial\Omega$. To obtain the dG discretization of (6), the set of piecewise-continuous, k-th degree, d-dimensional polynomial functions $\mathcal{V}_h^{d+2}$ is introduced

$$\mathcal{V}_h = \left\{\phi \in L_2\left(\Omega\right) : \phi|_K \in \mathbb{P}_d^k\left(K\right), \forall K \in \mathcal{K}_h\right\}. \tag{7}$$

Following Bassi et al. [17], an orthonormal and hierarchical basis $\{\phi\}_{l=1}^{N_{DoF}}$ $\forall K \in \mathcal{K}_h$ defined in the physical space is adopted for $\mathcal{V}_h$, where $N_{DoF} = \prod_{m=1}^{d}\left(k + m\right)/m$. Since the approximation is discontinuous across any face of a cell, the jump $[\![\circ]\!]$ and average $\{\circ\}$ operators are introduced to properly define the dG discretization.

To ensure that the spatial discretization is entropy conservative or entropy stable we adopt the methodology proposed in [11]. The solution is expressed in terms of the conservative variables $\mathbf{q}_h$, while the residual of the spatial discretization is evaluated from the L_2-projection of $\mathbf{q}_h$ on the entropy set $\mathbf{v}_h \in [\mathcal{V}_h]^{d+2}$. By replacing functions $\mathbf{q}$ and $\mathbf{\Phi}$ in Eq. (6) with discontinuous finite element approximation $\mathbf{q}_h, \mathbf{\Phi}_h \in [\mathcal{V}_h]^{d+2}$, the dG discretization of the governing equations results in the following semi-discrete system

$$\begin{aligned}\sum_{K\in\mathcal{K}_h}\int_K \phi_{h,l}\frac{dq_{h,\kappa}}{dt}d\Omega - \sum_{K\in\mathcal{K}_h}\int_K \frac{\partial\phi_{h,l}}{\partial x_i}F_{\kappa,i}\left(\mathbf{v}_h, \nabla\mathbf{v}_h + \mathbf{r}\left([\![\mathbf{v}_h]\!]\right)\right)d\Omega \\ + \sum_{F\in\mathcal{F}_h}\int_F [\![\phi_{h,l}]\!]\hat{F}_\kappa\left(\mathbf{v}_h^\pm, \left(\nabla_h\mathbf{v}_h + \eta_F\mathbf{r}_F\left([\![\mathbf{v}_h]\!]\right)\right)^\pm, \mathbf{n}_F\right)d\sigma = 0.\end{aligned} \tag{8}$$

Due to the orthogonality of the basis, the mass matrix in Eq.(8) corresponds to the identity. The sum of the convective and viscous flux functions, $\mathbf{F} = \mathbf{F}_c + \mathbf{F}_v$, is replaced at mesh faces by its numerical counterpart $\hat{\mathbf{F}}$. Convective numerical fluxes $\hat{\mathbf{F}}_c$ are evaluated using the entropy-stable Godunov flux computed from the exact Riemann solver of [18], except in explicitly stated entropy-conserving cases, where the entropy-conserving flux of Ranocha [19] is used instead. The viscous fluxes are discretized following the BR2 approach [20].

Strictly satisfying the discrete entropy balance requires exact integration which entails a remarkable computational overhead [21]. To circumvent this limitation, the discretization is augmented with the DEEB [14, 22]. Rather than relying on numerical over-integration, the DEEB applies an explicit, element-wise correction to the system, restoring the correct entropy behaviour. The final semi-discrete form reads

$$
\begin{aligned}
\sum_{K\in\mathcal{K}_h}\int_K \phi_{h,l}\frac{dq_{h,\kappa}}{dt}\,d\Omega - \sum_{K\in\mathcal{K}_h}\int_K \frac{\partial\phi_{h,l}}{\partial x_i}F_{\kappa,i}\left(\mathbf{v}_h,\nabla_h\mathbf{v}_h + \mathbf{r}\left(\llbracket\mathbf{v}_h\rrbracket\right)\right)d\Omega \\
+\sum_{F\in\mathcal{F}_h}\int_F \llbracket\phi_{h,l}\rrbracket\hat{F}_\kappa\left(\mathbf{v}_h^{\pm},\left(\nabla_h\mathbf{v}_h + \eta_F\mathbf{r}_F\left(\llbracket\mathbf{v}_h\rrbracket\right)\right)^{\pm},\mathbf{n}_F\right)d\sigma \\
+\sum_{K\in\mathcal{K}_h}\alpha_K\frac{\displaystyle\int_K \phi_{h,l}\,\bar{\mathbf{v}}_{h,\kappa}\,d\Omega}{\displaystyle\int_K \bar{\mathbf{v}}_h^{\top}\bar{\mathbf{v}}_h\,d\Omega} = 0,
\end{aligned}
\tag{9}
$$

where $\bar{\mathbf{v}}_h = \mathbf{v}_h - \mathbf{v}_{h,0}$ with $\mathbf{v}_{h,0}$ being the elemental mean value of $\mathbf{v}_h$, while α_K is a scalar coefficient quantifying the local elemental entropy defect [11]. Although the dG formulation is here presented for the compressible Navier–Stokes equations, the inviscid Euler case is recovered naturally by setting the viscous flux $\mathbf{F}_v$ to zero.

Since no implicit matrix inversion is involved, the system of Ordinary Differential Equations resulting from the numerical integration of Eq.(9) using suitable quadrature rules is

$$
\frac{d\mathbf{Q}}{dt} + \mathbf{R}\left(\mathbf{Q}\right) = \mathbf{0}, \tag{10}
$$

where $\mathbf{R}\left(\mathbf{Q}\right)$ is the residual vector arising from the spatial discretization. The semi-discrete system is then directly integrated in time using explicit Strong Stability Preserving Runge–Kutta (SSPRK) schemes [15]. In the present computations, the five-stage, fourth-order SSPRK scheme is adopted, leading to a robust and computationally efficient framework.

3. WMiLES implementation

The wall model is implemented as a boundary condition imposed at each wall quadrature point p_d. During the preprocessing phase, for every destination quadrature point p_d on a wall-modeled face, a corresponding donor point p_D must be identified along the wall-normal direction [23]. The selection of this exchange location is highly critical: sampling too close to the wall exposes the model to under-resolved solution, leading to the well-known log-layer mismatch [24]. To overcome this issue, following the recommendations of Frère et al. [25] for WMiLES within dG discretizations, the donor point p_D is located at the base, *i.e.*, the interior interface, of the second element from the wall. This strategy ensures that the sampled flow state is sufficiently decoupled from near-wall numerical errors, providing a well resolved input to the wall model. During the residual assembly, the local density ρ, kinematic viscosity ν, and the tangential velocity vector $\mathbf{u}_t = (\mathbf{I} - \mathbf{n}\otimes\mathbf{n})\,\mathbf{u}$, are reconstructed at p_D from the degrees of freedom of the second element from the wall. Here the wall-normal distance is computed as $y = \mathrm{dist}(p_D, p_d)$. The friction velocity u_τ is then obtained by solving a non-linear law-of-the-wall via a Newton-Raphson method

$$G(u_\tau) = \frac{|\mathbf{u}_t|}{u_\tau} - u^+(y^+) = 0, \tag{11}$$

where $y^+ = yu_\tau/\nu$ and the dimensionless velocity profile $u^+(y^+)$ is prescribed by the Reichardt law [26], as done in [23, 25]. The modeled wall shear stress follows directly as $\tau_w = \rho u_\tau^2$. For isothermal walls, once the wall shear stress is known, the wall normal heat flux q_w is explicitly determined through the Kader law [27], as presented in Le Bras et al. [28]. Finally, at the wall, the slip condition $\mathbf{u} \cdot \mathbf{n} = 0$ is enforced, and the viscous flux is properly modified to impose both the modeled shear stress τ_w and the heat flux q_w.

As an alternative to algebraic wall models, ODE-based ones have also been implemented, namely the equilibrium model for compressible flows proposed in Larsson et al. [29] and the non-equilibrium model of Kamogawa et al. [30]. In particular, taking advantage of the underlying numerical framework, we propose a dG discretization of these models. Here, for brevity, the dG discretization is described for the equilibrium ODE model, while the same procedure is applied to the Kamogawa model after recasting it in first-order form. A complete derivation of the one-dimensional dG formulation, including numerical fluxes, boundary-state construction and implementation details, will be reported in a forthcoming paper.

For each wall quadrature point p_d, a one-dimensional wall-normal mesh is generated during preprocessing between the wall point and the corresponding donor point p_D. The local coordinate is denoted by $y^{wm} \in [0, h_{ex}]$, where $y^{wm} = 0$ corresponds to the wall and $y^{wm} = h_{ex}$ to the exchange location. In order to increase the resolution close to the wall, the nodes of the one-dimensional mesh can be geometrically stretched through a user-defined stretching parameter r. Denoting by N_e^{wm} the number of one-dimensional elements, the interpolation factor associated with the n-th grid node, inspired by [31], is defined as

$$f_n = \begin{cases} \dfrac{n-1}{N_e^{wm}}, & r = 1, \\ \dfrac{r^{n-1} - 1}{r^{N_e^{wm}} - 1}, & r \neq 1, \end{cases} \qquad n = 1, \dots, N_e^{wm} + 1. \tag{12}$$

The coordinates of the one-dimensional grid nodes are then obtained by a linear mapping between the wall point and the donor point

$$y_n^{wm} = (1 - f_n)\, y^{wm}(0) + f_n\, y^{wm}(h_{ex}). \tag{13}$$

Therefore, $r = 1$ gives a uniform distribution, while $r > 1$ progressively clusters the nodes towards the wall. The wall-model solution is then obtained by solving an independent one-dimensional boundary-value problem along each wall-normal segment. In the equilibrium model, pressure-gradient effects and wall-normal convection are neglected inside the wall-modeled layer [29]. Introducing the total shear stress τ and the auxiliary heat-flux variable q, the second-order wall-model equations can be rewritten as the following first-order system

$$\begin{cases} \dfrac{dU}{dy} = \dfrac{\tau}{\mu_{\text{eff}}}, \\ \dfrac{d\tau}{dy} = 0, \\ \dfrac{dT}{dy} = -\dfrac{q}{K_{\text{eff}}}, \\ \dfrac{dq}{dy} = \dfrac{d(U\tau)}{dy}. \end{cases} \tag{14}$$

Here, U is the scalar velocity component along the local tangential direction $\mathbf{h}_t$. This direction is determined from the instantaneous LES velocity vector sampled at the donor point. Specifically, its projection onto the wall-tangent plane defines the tangential donor velocity vector $\mathbf{u}_t$, from which the unit vector is set as $\mathbf{h}_t = \mathbf{u}_t/|\mathbf{u}_t|$. The effective transport coefficients are defined as

$$\mu_{\text{eff}} = \mu + \mu_t, \qquad K_{\text{eff}} = c_p \left(\frac{\mu}{Pr} + \frac{\mu_t}{Pr_t} \right), \tag{15}$$

where μ_{t} is obtained from a mixing-length eddy-viscosity closure and $Pr_t = 0.9$ as proposed in [29]. The boundary conditions are imposed at the wall and at the exchange location as

$$U(0) = U_w, \qquad U(h_{ex}) = |\mathbf{u}_t|, \qquad T(0) = T_w, \qquad T(h_{ex}) = T_D. \tag{16}$$

In the present applications, $U_w = 0$ for a stationary wall, whereas $|\mathbf{u}_t|$ and T_D are obtained from the LES solution reconstructed at the donor point p_D.

The unknowns U_h, τ_h, T_h, and q_h are approximated in a discontinuous polynomial space $\mathcal{V}_h^{wm}$ of degree k_{wm}, defined on the one-dimensional wall-model mesh. The basis for $\mathcal{V}_h^{wm}$ is defined following [17]. After dG discretization and assembly over all wall-model elements, the problem is organized into two coupled algebraic subsystems. The first subsystem collects the degrees of freedom associated with the momentum-related variables, namely U_h and τ_h, whereas the second one collects those associated with the thermal variables, namely T_h and q_h. At each nonlinear iteration, the two subsystems are treated in segregated form using the latest available estimates of the thermodynamic state, the wall quantities, and the coupling terms. The corresponding algebraic operators depend on the effective transport properties and on the nonlinear interaction between the momentum-related and thermal wall-model fields. Since these quantities are state-dependent and coupled through the wall response, the segregated solution is embedded in an outer fixed-point, or Picard, iteration. At convergence, the wall shear stress and wall heat flux are extracted from the interior traces of the wall-model solution at the wall as $\tau_w = \tau_h(0^+)$, $q_w = q_h(0^+)$.

The same dG formulation is used for the non-equilibrium Kamogawa wall model. In that case, the governing ODE is first rewritten as a first-order system in the wall-normal coordinate and the corresponding additional source and coupling terms are included in the element residuals. The one-dimensional mesh, polynomial space and nonlinear iterative strategy remain the same as those described above for the equilibrium model. Since the Kamogawa wall model is for incompressible flows [30], once the wall shear stress is known the wall heat flux is explicitly determined from the Kader law.

4. Numerical results

The numerical assessment is organized in two parts. First, the inviscid Taylor–Green vortex is considered to verify the entropy conservation/stability properties of the numerical framework in a fully three-dimensional configuration. Then, the proposed implementation of WMiLES is evaluated on a turbulent channel flow at $Re_\tau = 2000$, for both algebraic wall model and dG-discretized equilibrium ODE wall model of [29].

4.1 Inviscid Taylor–Green vortex

The first numerical test is devoted to the assessment of the entropy conservation/stability properties of the numerical framework. To this end, we consider the weakly compressible inviscid Taylor–Green vortex, a three-dimensional benchmark commonly used to assess the numerical dissipation introduced by numerical schemes in under-resolved turbulent-flow simulations [32]. The initial condition is prescribed as

$$\begin{aligned}
u_1 &= U_0 \sin\left(\frac{x}{L}\right)\cos\left(\frac{y}{L}\right)\cos\left(\frac{z}{L}\right),\\
u_2 &= -U_0 \cos\left(\frac{x}{L}\right)\sin\left(\frac{y}{L}\right)\cos\left(\frac{z}{L}\right),\\
u_3 &= 0,\\
p &= p_0 + \frac{\rho_0 U_0^2}{16}\left[\cos\left(\frac{2x}{L}\right)+\cos\left(\frac{2y}{L}\right)\right]\left[\cos\left(\frac{2z}{L}\right)+2\right],\\
\rho &= \rho_0,
\end{aligned} \tag{17}$$

where $\rho_0 = 1$, $p_0 = 1$, $\gamma = 1.4$, and $U_0 = M_0\sqrt{\gamma}$, with $M_0 = 0.1$. The computational domain is the triply periodic cube $\Omega = [0, 2\pi L]^3$ with $L = 1$. Since the inviscid Euler equations are solved, no physical viscous dissipation is present and the evolution of the global entropy is only affected by the numerical discretization.

The quantity monitored in this test is the cumulative production of physical entropy,

$$\varepsilon_{\rho s}(t) = \frac{1}{|\Omega|}\left[\int_\Omega \rho s(\mathbf{x}, t)\; d\Omega - \int_\Omega \rho s_{\mathrm{prj}}(\mathbf{x}, 0)\; d\Omega\right], \tag{18}$$

where $s = \ln(p/\rho^\gamma)$ is the thermodynamic entropy and the subscript prj indicates that the reference value is set equal to the L_2-projection of the initial condition on the polynomial space. An entropy-conserving discretization should keep $\varepsilon_{\rho s}$ close to zero, whereas an entropy-stable discretization is expected to produce a non-negative entropy variation.

The domain is discretized using a mesh made of 4^3 curved hexahedral elements and polynomial degrees $k = \{3, 4, 5, 6\}$ are considered. The use of a curved mesh is meant to demonstrate the consistency of the entropy-aware dG framework in the presence of high-order geometrical mappings. For each polynomial degree, the entropy-conserving flux from Ranocha [19], denoted as EC, and the entropy-stable Godunov flux computed from the exact Riemann solver of [18], denoted as ES, are considered. The solution is advanced in time by imposing a maximum CFL number equal to 2.5×10^{-4}. Such a small time step is deliberately adopted in order to make the spurious entropy contribution associated with the explicit time integration negligible with respect to the entropy behaviour of the spatial discretization.

In Fig. 1 the time evolution of $\varepsilon_{\rho s}$ is shown for the considered polynomial degrees and fluxes. Solid lines denote ES simulations, whereas symbols denote EC simulations. The EC results collapse onto the zero-entropy-variation line at the scale of the figure, preserving the global physical entropy up to variations of the order of 10^{-13}. Such variations are compatible with round-off errors and with the residual contribution of the explicit time integration. This confirms that, for the present inviscid periodic test case, the DEEB-corrected entropy-projected formulation recovers the expected entropy-conserving behaviour when an EC flux is adopted. Conversely, the ES simulations show a monotone increase of $\varepsilon_{\rho s}$, consistently with the interface dissipation introduced by the exact Riemann solver.

The comparison among polynomial degrees further highlights the role of the spatial resolution. For the ES cases, the amount of entropy production depends on k, since increasing the polynomial degree modifies the resolved portion of the flow spectrum and, consequently, the amount of energy dissipated by the numerical flux. On the other hand, the EC results remain clustered close to zero for all the considered

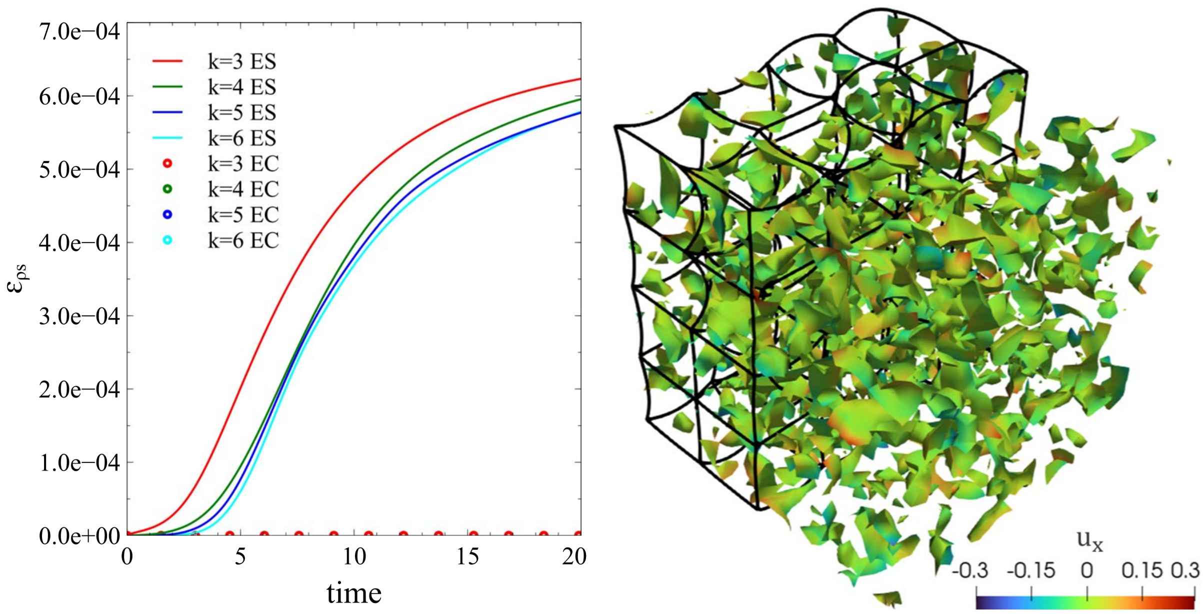

Figure 1: Inviscid Taylor–Green vortex on a 4^3 curved hexahedral mesh. Left: time evolution of $\varepsilon_{\rho s}$ for $k = \{3, 4, 5, 6\}$. Right: instantaneous isosurface of the Q-criterion for $Q = 0.02$ at $t = 20$ for $k = 6$, coloured by the velocity component u_x; the computational mesh is also shown.

values of k, showing that the conservation property is not affected by the polynomial degree in the present setup.

Figure 1 also shows, for $k = 6$, an instantaneous isosurface of the Q-criterion at the final simulation time $t = 20$, coloured by the velocity component u_x. The computational mesh is also displayed to highlight both the coarse spatial discretization and the use of curved hexahedral elements. This visualization qualitatively illustrates the vortical structures generated by the Taylor–Green vortex breakdown and confirms that the entropy analysis is performed in an under-resolved flow configuration on a non-affine high-order mesh.

4.2 Turbulent channel flow at $Re_\tau = 2\,000$

The second numerical test is devoted to the assessment of the proposed WMiLES implementation in a canonical wall-bounded turbulent configuration. We consider a plane turbulent channel flow at friction Reynolds number $Re_\tau = 2\,000$ in the near-incompressible regime, with $M = 0.002$ based on the friction velocity u_τ. The computational domain is $\Omega = [0, 2\pi\delta] \times [0, 2\delta] \times [0, \pi\delta]$, where δ is the channel half-height. Periodic boundary conditions are imposed in the streamwise and spanwise directions, while the isothermal wall-model boundary condition described in Sec. 3 is imposed at the two walls. The flow is driven by a constant pressure-gradient forcing term added to the x-momentum equation.

The computational mesh is made of $20 \times 10 \times 10$ uniform hexahedral elements in the streamwise, wall-normal and spanwise directions, respectively, as in [25]. Since $\delta = 1$, the wall-normal element size is $\Delta y = 0.2\delta$. Therefore, following the donor-point selection strategy introduced in Sec. 3, the exchange location is placed at $y = 0.2\delta$ from the wall. This value is consistent with the donor-location recommendation of Frère et al. [25] for wall-modeled dG simulations.

Two wall-modeling strategies are considered. The first one is the algebraic wall model based on the Reichardt and Kader laws. The second one is the dG-discretized equilibrium ODE wall model for compressible flows of Larsson et al. [29]. For the ODE-based computations, the one-dimensional wall-model problems are solved using the strategy described in Sec. 3. In particular, each wall-normal segment is discretized with $N_e^{wm} = 30$ elements and polynomial degree $k_{wm} = 3$. The geometric stretching parameter introduced in Eq. (12) is set to $r = 1.1$, providing a mild clustering of the wall-model nodes towards the wall.

The mean streamwise velocity is represented in wall units $u^+ = \langle u \rangle / u_\tau$ and $y^+ = y u_\tau / \nu_w$ where u_τ is the friction velocity, ν_w is the wall kinematic viscosity, and $\langle \cdot \rangle$ denotes averaging over the statistically homogeneous directions and time. The numerical results are compared with the DNS data of Hoyas and Jiménez [33] and the logarithmic law $u^+ = \ln (y^+) / \kappa + B$, with $\kappa = 0.41$ and $B = 5.2$. For visualization purposes, the profiles corresponding to different polynomial degrees are vertically shifted in the plots of $\Delta u^+ = 4$.

The results are summarized in Fig. 2, where the left column refers to the algebraic wall model and the right column to the dG-discretized equilibrium ODE wall model. The first and second rows show the complete mean-velocity profile and a detailed view of the logarithmic and outer regions, respectively.

The algebraic wall-model results are shown for polynomial degrees $k = \{4, 5, 6, 7\}$. As expected for a wall-modeled computation performed on a very coarse wall-normal grid, the largest discrepancy with respect to the DNS reference is observed inside the first wall-adjacent element, where the inner part of the boundary layer is not resolved. From the donor location onward, the computed mean-velocity profiles show a reasonable agreement with the reference data. Increasing the polynomial degree improves the effective resolution inside each element and generally leads to a better reconstruction of the mean profile.

For the highest polynomial degree considered here, namely $k = 7$, the mean velocity profile exhibits a slight shift when approaching the channel centre. Although the effect remains limited, it may reflect a sensitivity to the numerical dissipation provided by the scheme, which acts as the subgrid-scale dissipation in the present WMiLES framework. A more detailed assessment of this point is left to future work.

The corresponding results for the ODE wall model are presented for polynomial degrees $k = \{4, 5, 6\}$. As expected, the mean-velocity profiles are very close to those obtained with the algebraic wall model; this behaviour is consistent with the equilibrium nature of the channel-flow configuration, where non-equilibrium effects are absent. In this setting, the ODE wall model reconstructs an equilibrium wall-normal profile and therefore leads to mean-flow predictions very similar to those obtained with the algebraic law.

Overall, the comparison confirms that both wall-modeling strategies have been correctly integrated into the entropy-aware dG framework. The algebraic and ODE-based models exhibit the same qualitative trend with polynomial-degree refinement and provide similar predictions for the mean velocity. The results therefore provide a first validation of the proposed WMiLES strategy on a high-Reynolds-number wall-bounded turbulent flow.

5. Conclusion and Future Work

In this work, we have presented the current status of the implementation of wall-modeling strategies within an entropy-aware modal discontinuous Galerkin solver for the compressible Navier–Stokes equations. The proposed WMiLES formulation replaces the no-slip wall condition with a slip condition coupled with modeled wall shear stress and heat flux contributions. Both algebraic wall laws and ODE-based wall models have been considered, the latter being discretized through a one-dimensional dG formulation along wall-normal segments connecting each wall quadrature point to its donor location.

The inviscid Taylor–Green vortex was first considered to demonstrate that the underlying dG discretization exhibits the expected entropy-conserving/stable behaviour. Preliminary WMiLES results have then been presented for a turbulent channel flow at $Re_\tau = 2\,000$ on a very coarse uniform mesh. The computed mean velocity profiles show reasonable agreement with DNS data from the donor location onward, and the algebraic and equilibrium ODE wall models provide comparable trends, supporting the correct integration of both strategies within the solver.

The present results represent a first step toward a complete validation of the proposed WMiLES framework.

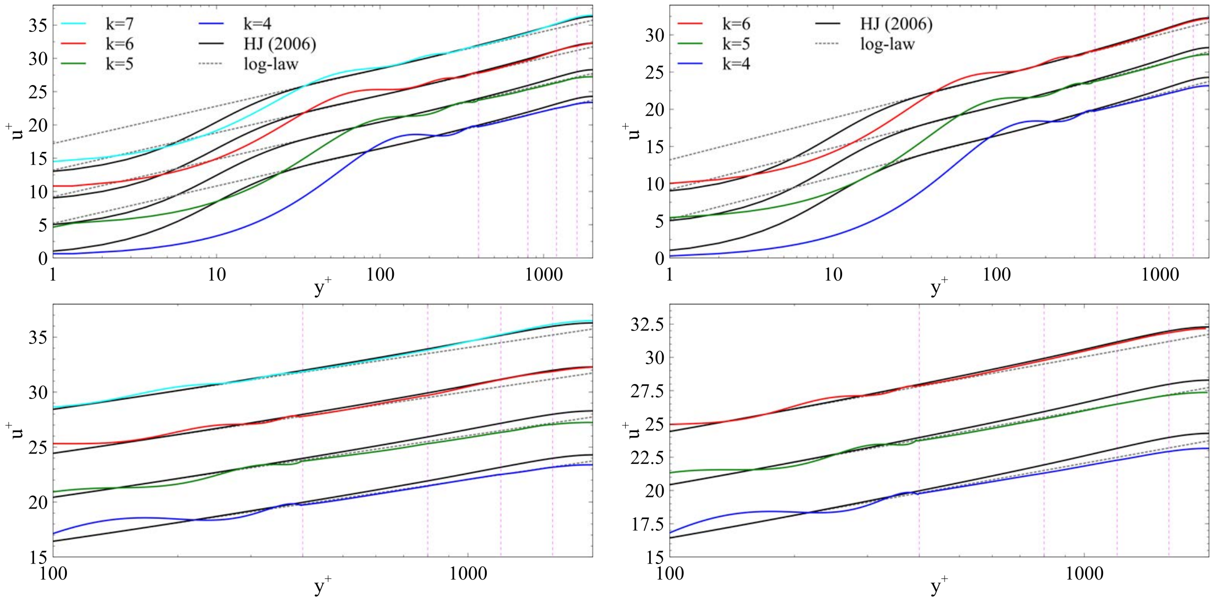

Figure 2: Turbulent channel flow at $Re_\tau = 2000$ on a $20\times10\times10$ uniform hexahedral mesh. Left column: algebraic wall model. Right column: dG-discretized equilibrium ODE wall model of [29]. First row: complete mean streamwise velocity profiles. Second row: detail of the logarithmic and outer regions. DNS data from Hoyas and Jiménez (HJ) [33] are reported as reference; the logarithmic law is also shown. Vertical magenta dashed lines indicate the elements interfaces.

Future developments will include a more systematic analysis of the sensitivity to the donor-point location and to the discretization parameters. In addition, the use of non-equilibrium ODE wall models in pressure-gradient and separated-flow configurations will be investigated.

Acknowledgements

Alessandro Colombo, Francesco Carlo Massa and Francesco Mangini acknowledge ROSAS "RObust simulation Systems exploiting AI-based turbulence models and high-fidelity algorithms" Horizon Europe project (GA 101138319).

Funded by the European Union. Views and opinions expressed are, however, those of the author(s) only and do not necessarily reflect those of the European Union. Neither the European Union nor the granting authority can be held responsible for them.

Funded by the European Union

References

[1] N. Ashton and W. van Noordt. Overview and summary of the first Automotive CFD prediction workshop: DrivAer Model. *SAE International Journal of Commercial Vehicles*, 2022.

[2] H. Choi and P. Moin. Grid-point requirements for Large Eddy Simulation: Chapman's estimates revisited. *Physics of Fluids*, 24(1):011702, 01 2012.

[3] U. Piomelli. Wall-layer models for large-eddy simulations. *Progress in Aerospace Sciences*, 44(6):437–446, 2008.

[4] H. Owen, G. Chrysokentis, M. Avila, D. Mira, G. Houzeaux, R. Borrell, J. C. Cajas, and O. Lehmkuhl. Wall-Modeled Large-Eddy simulation in a finite element framework. *International Journal for Numerical Methods in Fluids*, 92(1):20–37, 2020.

[5] Y. Lv, X. I. A. Yang, G. I. Park, and M. Ihme. A discontinuous Galerkin method for Wall-Modeled Large-Eddy Simulations. *Computers & Fluids*, 222:104933, 2021.

[6] A. Frère, K. Hillewaert, P. Chatelain, and G. Winckelmans. High Reynolds number airfoil: From Wall-Resolved to Wall-Modeled LES. *Flow, Turbulence and Combustion*, 101(2):457–476, 2018.

[7] A. Amatriain, C. Gargiulo, and G. Rubio. Generalized Wall-Modeled Large Eddy Simulation model for industrial applications. *Physics of Fluids*, 36(1):015141, 01 2024.

[8] F. Bassi, L. Botti, A. Colombo, A. Crivellini, A. Ghidoni, and F. Massa. On the development of an implicit high-order discontinuous Galerkin method for DNS and implicit LES of turbulent flows. *European Journal of Mechanics, B/Fluids*, 55:367–379, jan 2016.

[9] B. F. Klose, E. J. Munoz Lopez, A. Hergt, J. Klinner, M. Bergmann, and C. Morsbach. Analysis of a transonic cascade with Wall-Modeled LES based on DGSEM. In *Direct and Large Eddy Simulation XIII*, volume 31 of *ERCOFTAC Series*, pages 157–163. Springer, 2024.

[10] B. Cockburn and C.-W. Shu. The Runge–Kutta discontinuous Galerkin Method for conservation laws V: Multidimensional Systems. *Journal of Computational Physics*, 141(2):199–224, 1998.

[11] L. Alberti, E. Carnevali, A. Colombo, and A. Crivellini. An entropy conserving/stable discontinuous Galerkin solver in entropy variables based on the direct enforcement of entropy balance. *Journal of Computational Physics*, 508:113007, 2024.

[12] L. Alberti, F. Bassi, E. Carnevali, A. Colombo, A. Crivellini, and A. Nigro. A comparative study of different sets of variables in a discontinuous Galerkin method with Entropy Balance Enforcement. *International Journal of Computational Fluid Dynamics*, 37(6):487–508, 2023.

[13] J. Chan, H. Ranocha, A. M. Rueda-Ramírez, G. Gassner, and T. Warburton. On the entropy projection and the robustness of high order entropy stable discontinuous Galerkin schemes for under-resolved flows. *Frontiers in Physics*, Volume 10 - 2022, 2022.

[14] R. Abgrall. A general framework to construct schemes satisfying additional conservation relations. application to entropy conservative and entropy dissipative schemes. *Journal of Computational Physics*, 372:640–666, 2018.

[15] R. J. Spiteri and S. J. Ruuth. A new class of optimal high-order strong-stability-preserving time discretization methods. *SIAM Journal on Numerical Analysis*, 40(2):469–491, 2002.

[16] G. Lodato, P. Castonguay, and A. Jameson. Structural Wall-Modeled LES using a high-order spectral difference scheme for unstructured meshes. *Flow, Turbulence and Combustion*, 92(1-2):579–606, 01 2014.

[17] F. Bassi, L. Botti, A. Colombo, D. A. Di Pietro, and P. Tesini. On the flexibility of agglomeration based physical space discontinuous Galerkin discretizations. *Journal of Computational Physics*, 231(1):45–65, Sep 2011.

[18] J. J. Gottlieb and C. P. T. Groth. Assessment of Riemann solvers for unsteady one-dimensional inviscid flows of perfect gases. *Journal of Computational Physics*, 78(2):437–458, oct 1988.

[19] H. Ranocha. Entropy conserving and kinetic energy preserving numerical methods for the Euler equations using summation-by-parts operators. In S. J. Sherwin, D. Moxey, J. Peiró, P. E. Vincent, and C. Schwab, editors, *Spectral and High Order Methods for Partial Differential Equations ICOSAHOM 2018*, pages 525–535. Springer International Publishing, 2020.

[20] F. Bassi and S. Rebay. A high-order accurate discontinuous Finite Element Method for the numerical solution of the compressible Navier–Stokes equations. *Journal of Computational Physics*, 131(2):267–279, 1997.

[21] A. Colombo, A. Crivellini, and A. Nigro. Entropy conserving implicit time integration in a discontinuous Galerkin solver in entropy variables. *Journal of Computational Physics*, 472:111683, 2023.

[22] R. Abgrall, P. Öffner, and H. Ranocha. Reinterpretation and extension of entropy correction terms for residual distribution and discontinuous Galerkin schemes: Application to structure preserving discretization. *Journal of Computational Physics*, 453:110955, 03 2022.

[23] R. Hartmann. Wall-resolved and Wall-Modeled iLES based on high-order dG. In R. Owen, R. de Borst, J. Reese, and C. Pearce, editors, *6th European Conference on Computational Mechanics, ECCM 2018 and 7th European Conference on Computational Fluid Dynamics, ECFD 2018*, pages 4194–4207, 2019.

[24] S. Kawai and J. Larsson. Wall-modeling in Large Eddy Simulation: Length scales, grid resolution, and accuracy. *Physics of Fluids*, 24(1):015105, 01 2012.

[25] A. Frère, C. Carton de Wiart, K. Hillewaert, P. Chatelain, and G. Winckelmans. Application of wall-models to discontinuous Galerkin LES. *Physics of Fluids*, 29(8):085111, 08 2017.

[26] H. Reichardt. Vollständige Darstellung der turbulenten geschwindigkeits- verteilung in glatten leitungen. *ZAMM - Zeitschrift für Angewandte Mathematik und Mechanik*, 31:208–219, 1951.

[27] B. A. Kader. Temperature and concentration profiles in fully turbulent boundary layers. *International Journal of Heat and Mass Transfer*, 24(9):1541–1544, 1981.

[28] S. Le Bras, H. Deniau, C. Bogey, and G. Daviller. Development of compressible large-eddy simulations combining high-order schemes and Wall Modeling. *AIAA Journal*, 55(4):1152–1163, 2017.

[29] J. Larsson, S. Kawai, J. Bodart, and I. Bermejo-Moreno. Large Eddy Simulation with modeled wall-stress: recent progress and future directions. *Mechanical Engineering Reviews*, 3(1):15–00418–15–00418, 2016.

[30] R. Kamogawa, Y. Tamaki, and S. Kawai. Ordinary-differential-equation-based nonequilibrium wall modeling for large-eddy simulation. *Phys. Rev. Fluids*, 8:064605, Jun 2023.

[31] E. Gillyns, S. Buckingham, and G. Winckelmans. Implementation and validation of an algebraic Wall Model for LES in Nek5000. *Flow, Turbulence and Combustion*, 109(4):1111–1131, 2022.

[32] C.-W. Shu, W. S. Don, D. Gottlieb, O. Schilling, and L. Jameson. Numerical convergence study of nearly incompressible, inviscid Taylor–Green Vortex flow. *J. Sci. Comput.*, 24:1–27, 07 2005.

[33] S. Hoyas and J. Jiménez. Scaling of the velocity fluctuations in turbulent channels up to $Re_\tau = 2003$. *Physics of Fluids*, 18(1):011702, 2006.